Zhou, S.; William, A.; Lintner, B.; Berg, A.; Zhang, Y.; Keenan, T.; Cook, B.; Hagemann, S.; Seneviratne, S.; Gentine, P.:
Soil moisture–atmosphere feedbacks mitigate declining water availability in drylands.
In: Nature Climate Change. Vol. 11 (2021) 38 - 44.
First published online by Nature Publishing Group: 04.01.2021

https://dx.doi.org/10.1038/s41558-020-00945-z

Soil moisture-atmosphere feedbacks mitigate declining water availability in drylands

Sha Zhou[1,2,3,4,5*], A. Park Williams[1], Benjamin R. Lintner[6], Alexis M. Berg[7], Yao Zhang[4,5], Trevor F. Keenan[4,5], Benjamin I. Cook[1,8], Stefan Hagemann[9], Sonia I. Seneviratne[10], Pierre Gentine[2,3]

[1]Lamont-Doherty Earth Observatory of Columbia University, Palisades, NY, USA

[2]Earth Institute, Columbia University, New York, NY, USA

[3]Department of Earth and Environmental Engineering, Columbia University, New York, NY, USA

[4]Climate and Ecosystem Sciences Division, Lawrence Berkeley National Laboratory, Berkeley, CA, USA

[5]Department of Environmental Science, Policy and Management, UC Berkeley, Berkeley, CA, USA

[6]Department of Environmental Sciences, Rutgers, The State University of New Jersey, New Brunswick, NJ, USA

[7]Department of Earth and Planetary Sciences, Harvard University, Cambridge, MA, USA

[8]NASA Goddard Institute for Space Studies, New York, NY, USA

[9]Helmholtz-Zentrum Geesthacht, Institute of Coastal Research, Geesthacht, Germany

[10]Institute for Atmospheric and Climate Science, ETH Zurich, Zurich, Switzerland

*Correspondence to: sz2766@columbia.edu

Global warming alters surface water availability (precipitation minus evapotranspiration, P-E) and hence freshwater resources. However, the influence of land-atmosphere feedbacks on future P-E changes and the underlying mechanisms remain unclear. Here we demonstrate that soil moisture (SM) strongly impacts future P-E changes, especially in drylands, by regulating evapotranspiration and atmospheric moisture inflow. Using modeling and empirical approaches, we find a consistent negative SM feedback on P-E, which may offset ~60% of the decline in dryland P-E otherwise expected in the absence of SM feedbacks. The negative feedback is not caused by atmospheric thermodynamic responses to declining SM, but rather reduced SM, in addition to limiting evapotranspiration, regulates atmospheric circulation and vertical ascent to enhance moisture transport into drylands. This SM effect is a large source of uncertainty in projected dryland P-E changes, underscoring the need to

better constrain future SM changes and improve representation of SM-atmosphere processes in models.

Future changes in water availability pose great challenges to global freshwater and food security and the sustainability of natural ecosystems[1,2]. Changes in precipitation and evapotranspiration are especially important for dryland ecosystems where vegetation growth and mortality largely depend on water availability[3,4]. Global warming is expected to intensify the global water cycle[5–7], but the projected changes in surface water availability, namely precipitation minus evapotranspiration (P-E), exhibit divergent spatial patterns between ocean and land[8,9]. Over the ocean, projected P-E changes broadly follow the "dry-get-drier, and wet-get-wetter" (DDWW) paradigm, driven by increasing atmospheric moisture content and transport by the mean circulation in a warming climate[5,6]. However, thermodynamic mechanisms cannot effectively explain P-E changes over land, where the magnitudes of the P-E response to warming are much smaller than over the ocean[8,9]. Circulation anomalies driven by sea surface temperature changes have been demonstrated to cause deviations from the "wet-get-wetter" response in the wet tropics[10–12], but the dynamic mechanisms of dryland P-E changes, and their potential dependence on land surface feedbacks, are not well understood.

In water-limited regions, soil moisture (SM) directly regulates evapotranspiration, which may positively feed back onto precipitation via moisture recycling[13,14]. SM may also impact precipitation through its influence on boundary layer dynamics and mesoscale circulations[15–18]. For example, spatial gradients in SM and associated sensible heat flux gradients may preferentially promote convection over drier soils relative to surrounding wetter soils, resulting in a negative SM feedback on precipitation[15,18,19]. However, the sign of the SM-precipitation feedback can change in the presence of a background wind that enables the propagation of convective cells to neighboring regions[20]. Given that various processes may lead to short-term SM-precipitation feedbacks of opposing sign and/or varying strength, it is challenging to extrapolate the effects of these processes to longer timescales. The long-term (climatological) SM effects on P-E have yet to be diagnosed, particularly under future global warming.

Here we directly assess the long-term SM effect on future model-projected P-E using four general circulation models included in the Global Land Atmosphere Coupling Experiment (GLACE)-CMIP5[21] as well as simulations from 35 general circulation models in CMIP5 (Methods and Table S1). We quantify the SM contribution to P-E changes between 30-year historical (1971-2000) and future (2071-2100, RCP8.5) periods using three sets of model experiments in GLACE-CMIP5: a reference simulation (REF) with SM fully interactive with the atmosphere, and two perturbation simulations where SM climatology is prescribed as the 1971-2000 climatology (expA) and a centered, 30-year running mean climatology from REF (expB) (Extended Data Fig. 1). For each of the four models, the three simulations are driven by the same forcing agents (i.e., sea surface temperatures, sea ice, land use, and CO_2 concentrations), allowing us to compare them to isolate the total SM effect (REF-expA) and the effects of SM trends (expB-expA) and variability (REF-expB) on P-E changes. We further develop a multiple linear regression model to assess the sign and strength of the SM-(P-E) feedback and identify the primary feedback pathways by comparing SM effects on atmospheric dynamic and thermodynamic processes using two observationally constrained reanalysis products (MERRA-2 and ERA5) that provide pressure level, wind and humidity data in recent decades (1979-2018). These pressure level data are not available in GLACE-CMIP5.

Soil moisture effect on P-E changes in model projections

The 35 CMIP5 models show significant ($p<0.05$, Student's t-test) P-E increases in 42% of wet regions and P-E declines in 51% of dry regions over ocean between the historical and future periods (Fig. 1a and Extended Data Fig. 2e). Over land, future P-E is projected to increase significantly ($p<0.05$) in high-latitude wet regions, but its change is insignificant over 93% of dry regions. Here "dry" versus "wet" regions are characterized as negative versus positive P-E over ocean, and drylands versus non-drylands over land (Methods and Extended Data Fig. 2a-d). Unlike P-E changes, significant ($p<0.05$) SM changes are projected over 33% of drylands (Fig. 1b). Such SM changes directly impact evapotranspiration and may potentially feed back onto precipitation, both of which are expected to play a role in the projected P-E changes over land.

The spatial patterns of P-E and SM changes in REF of the four GLACE-CMIP5 models are largely consistent with the broader suite of CMIP5 models (Fig. 1a-d and Extended Data Fig. 2e,f), with spatial correlation coefficients of 0.82 for P-E over all grid cells and 0.35 for SM. In expA, in which the mean annual cycle of SM over the historical period is imposed throughout the entire simulation, the DDWW paradigm holds over 31% of the land regions, compared to only 19% of land areas showing DDWW in REF (Fig. 1c,e and Extended Data Fig. 2f,g). In particular, the proportion of drylands showing significant P-E declines in expA (30%) is three times that in REF (10%). Since P-E changes in expA are driven by factors excluding SM trends and variability, such as temperature-driven oceanic and atmospheric changes, we denote these factors collectively as non-SM effects.

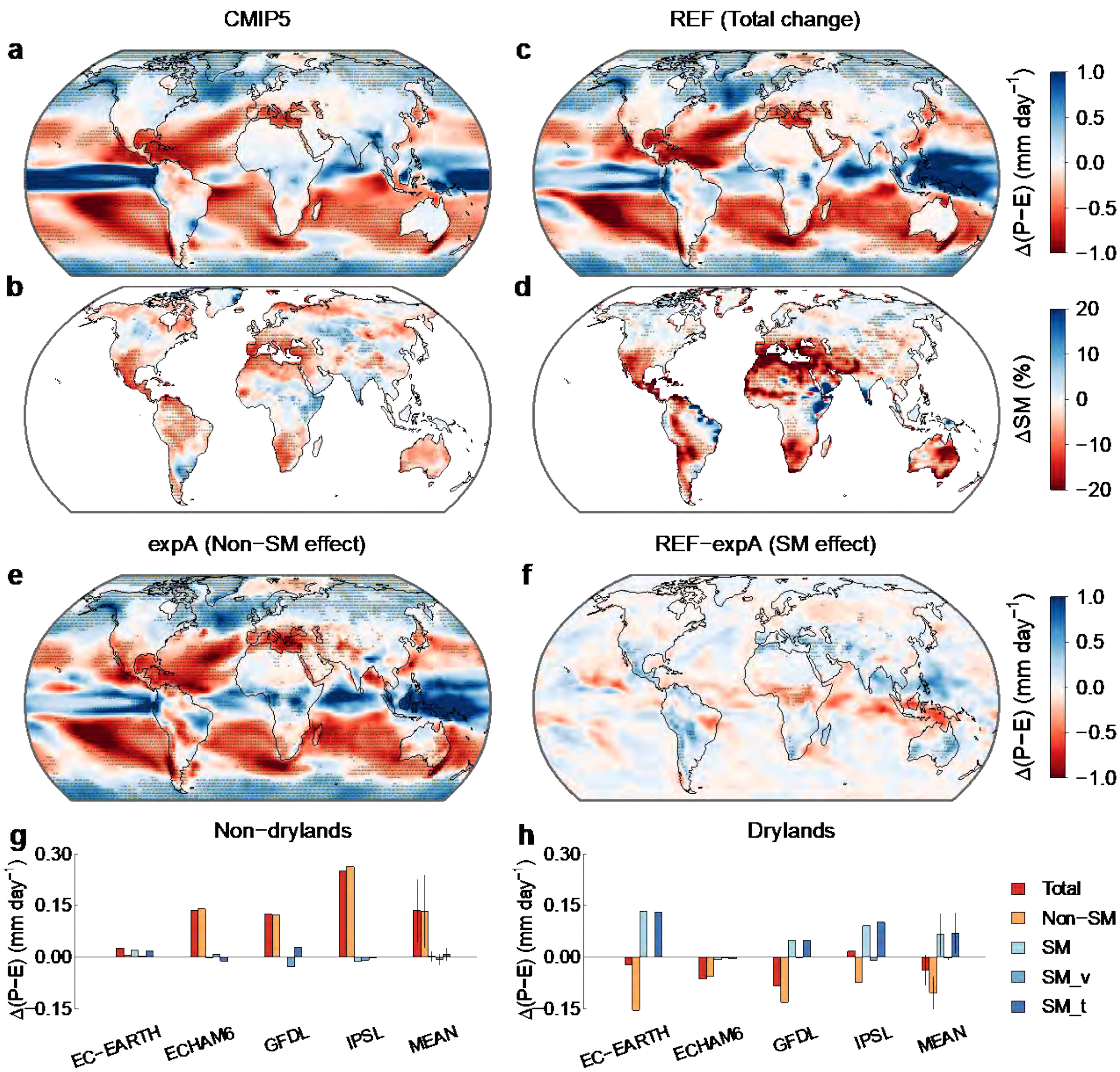

Fig. 1 | Multi-model mean annual changes in surface water availability and soil moisture. a-

b, Changes in precipitation minus evapotranspiration (Δ(P-E)) and percent changes in total soil moisture (ΔSM) between historical (1971-2000) and future (2071-2100, RCP8.5) periods (future minus historical values) in 35 CMIP5 models. **c**-**f**, The same as **a**-**b**, but for REF of the four GLACE-CMIP5 models (**c**-**d**), and Δ(P-E) induced by non-SM factors (expA, **e**) and SM (REF-expA, **f**). **g**-**h**, Total area-weighted Δ(P-E) and the contributions from non-SM factors, total SM changes, SM variability (SM_v), and SM trends (SM_t) across non-drylands (**g**) and drylands (**h**) in the four GLACE-CMIP5 models. The error bar shows the standard deviation of Δ(P-E) across the four models. Stippling denotes regions where the change in P-E is significant at the 95% level (Student's t-test) and the sign of the change is consistent with the sign of multi-model means (as shown in the figure) in at least 21 of the 35 (60%) CMIP5 models (**a**-**b**), and at least three of the four GLACE-CMIP5 models (**c**-**f**).

On the other hand, we isolate the SM effect on projected P-E changes by differencing the REF and expA simulations. The SM effects on projected P-E changes over land generally oppose the non-SM effects in expA (Fig. 1e,f), with spatial correlation coefficients ranging from -0.40 to -0.69 across the four models. The future SM changes and the P-E changes induced by SM are of opposite sign for multi-model means (Fig. 1d,f), and for each model (Extended Data Fig. 3) and season (Extended Data Fig. 4), indicating a negative SM feedback on P-E. P-E changes induced by non-SM factors are partially cancelled by the negative SM feedback on P-E, especially in drylands, where the SM-induced P-E increases in REF (0.066±0.060 mm/day, mean±1s.d.) offset 63% of the P-E declines (-0.104±0.046 mm/day) that would be otherwise induced by the non-SM factors simulated in expA (Fig. 1h). This offset effect is dominated by the negative SM trends over drylands (Fig. 1d), with minimal effect from changes in higher-frequency SM variability (Fig. 1h). The mitigating effect of declining SM on dryland P-E reduction is large in EC-EARTH (85%), GFDL (37%) and IPSL (123%), but no such effect is found in ECHAM6 because this model projects increased SM that reduces P-E in many tropical drylands (Extended Data Fig. 3b,f,j). Outside of drylands, P-E changes are generally dominated by non-SM factors (Fig. 1g).

Comparing the SM effects on precipitation and evapotranspiration, the decline in evapotranspiration (-0.163±0.083 mm/day) induced by future SM drying is roughly twice as large as the SM drying effect on precipitation (-0.097±0.052 mm/day) over drylands (Extended Data

Fig. 5). This stronger SM limitation on evapotranspiration than on precipitation indicates that the positive feedback of SM on precipitation via moisture recycling—or lower precipitation with future SM decline—is partially offset by other atmospheric responses to SM, as we discuss further in the following section.

Mechanisms of the soil moisture impact on P-E changes

Multiple theories have been postulated to explain future P-E changes over land, many of which focus on thermodynamic mechanisms, including warming-driven changes in specific humidity and land-ocean warming contrast[22–24]. Circulation changes, such as shifts in the strength of Walker and Hadley circulations, are also invoked to explain deviations of P-E changes from expected thermodynamic responses over land[10–12,25–28], but these dynamic mechanisms are predominantly driven by sea surface warming. Our finding of a strong SM effect on future P-E changes is not readily explained by these mechanisms. A recent study proposed an extended thermodynamic scaling of P-E changes including both local specific humidity changes and the horizontal gradient of specific humidity, but this extended scaling tends to overestimate both P-E decreases in drylands and P-E increases in the wet tropics[9], similar to the projected P-E changes by ocean-atmosphere processes in expA (Fig. 1e). This indicates that the thermodynamic effect does not fully capture the SM effect on P-E changes; rather, dynamic effects related to SM are necessary to account for these changes.

To test this hypothesis, we explore the thermodynamic and dynamic mechanisms of P-E changes driven by long-term SM trends in GLACE-CMIP5. Relative to expA, which lacks long-term SM trends, expB manifests greater temperature increases but weaker specific humidity increases (Fig. 2a-d). The SM effect is especially strong over drylands where negative trends in SM lead to reduced evapotranspiration and evaporative cooling (Extended Data Fig. 5b), which are consistent with the enhanced warming and reduced moistening in expB compared to expA (Fig. 2a-d). An SM-induced horizontal gradient of specific humidity is expected to induce more moisture into drylands by landward moisture flux, according to the extended thermodynamic scaling of P-E changes[9]. However, this negative effect may be partially or totally offset by local specific humidity reductions.

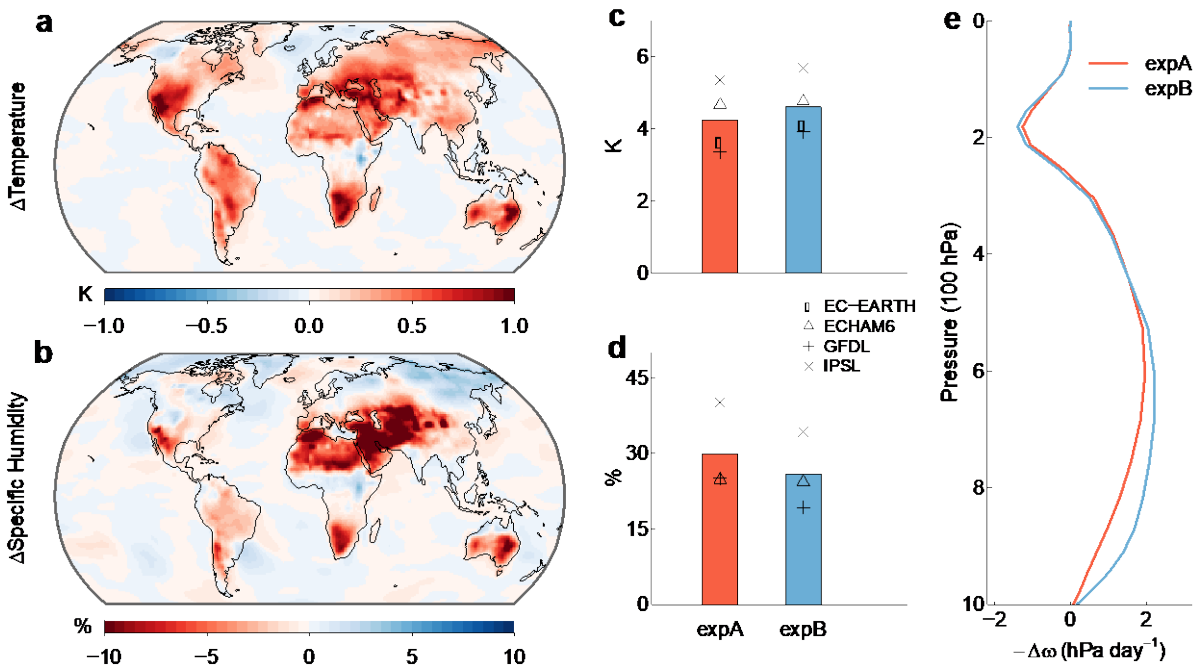

Fig. 2 | Soil moisture effects on changes in temperature, specific humidity, and vertical ascent in GLACE-CMIP5. a,**b**, Multi-model mean soil moisture effects (expB-expA) on projected changes (Δ) in temperature and specific humidity from historical (1971-2000) to future (2071-2100) periods (future minus historical values). **c**,**d**, Projected changes in temperature and specific humidity over drylands in expA and expB (bars: multi-model mean, symbols: individual models, specific humidity is not available in EC-EARTH). Changes to specific humidity are expressed fractionally relative to their historic period values (in percentages). **e**, Projected changes in negative pressure velocity (-Δω) over drylands in expA and expB for the IPSL model.

We examine the SM impact on atmospheric dynamic processes by comparing future changes in the vertical profile of vertical motion (here quantified in terms of -ω, the negative pressure velocity) over drylands between expA and expB in the IPSL model. Both simulations project enhanced ascent throughout the lower troposphere over drylands in the future, which is of greater magnitude in expB compared to expA (Fig. 2e). In particular, the SM effect on future P-E changes is largely consistent with that on tropospheric vertical ascent, with spatial correlation coefficients ranging from 0.37 to 0.59 over drylands (Extended Data Fig. 6). In each season, the spatial pattern of the SM effect on vertical ascent is also positively correlated with that on future P-E changes over drylands, especially in summer (wet season) (Extended Data Fig. 7). Although the SM effects on vertical ascent and P-E vary seasonally/geographically and across models, the IPSL results support the notion that reduced SM may promote atmospheric vertical ascent, potentially contributing to the negative SM effect on P-E.

Thermodynamic vs dynamic effects in the SM-(P-E) feedback

To further compare the thermodynamic and dynamic mechanisms of the negative SM-(P-E) feedback, we analyze the SM impact on the atmospheric moisture budget from the observationally constrained MERRA-2 and ERA5 reanalysis products. We apply a statistical framework to identify the SM feedback on P-E at the monthly scale, and to isolate the SM effects on the thermodynamic and dynamic components of P-E variations. We establish a multiple linear regression model to determine the sign and strength of the SM-(P-E) feedback, which is represented by a sensitivity coefficient that measures the partial derivative of standardized P-E variations to standardized SM variations in the previous month (Methods). A sensitivity coefficient of 0.1 indicates that P-E increases by 10% of its standard deviation when previous-month SM increases by one standard deviation.

Consistent with the experimental results in Fig. 1, we find widespread negative sensitivity coefficients for SM→(P-E), i.e., the effect of SM on P-E, in the fully coupled simulations of GLACE-CMIP5 models and reanalysis products, with significant effects in the subtropical and mid-latitude dry regions (Fig. 3a,d,g). We further compare SM→E and SM→P. As expected, SM exerts a strong positive impact on evapotranspiration, while its effect on precipitation is much weaker (Fig. 3b,c,e,f,h,i), because precipitation is strongly controlled by large-scale atmospheric dynamics. We note that the strengths of SM→E and SM→P vary across models and reanalysis products (Fig. 3c,f,i). In addition to intrinsic differences in the representation of land-atmosphere processes, different treatments of vegetation dynamics and our use of different soil depths across models/products may also contribute to uncertainties in the feedback strengths (Methods). Besides evapotranspiration, atmospheric moisture convergence (MC) is the other source of moisture for precipitation. We find consistent negative SM→MC in MERRA-2 and ERA5 (Fig. 3j,m). As monthly SM variations strongly and positively force evapotranspiration but generally negatively affect moisture convergence, SM has a more muted effect on precipitation than on evapotranspiration, resulting in a negative SM-(P-E) feedback.

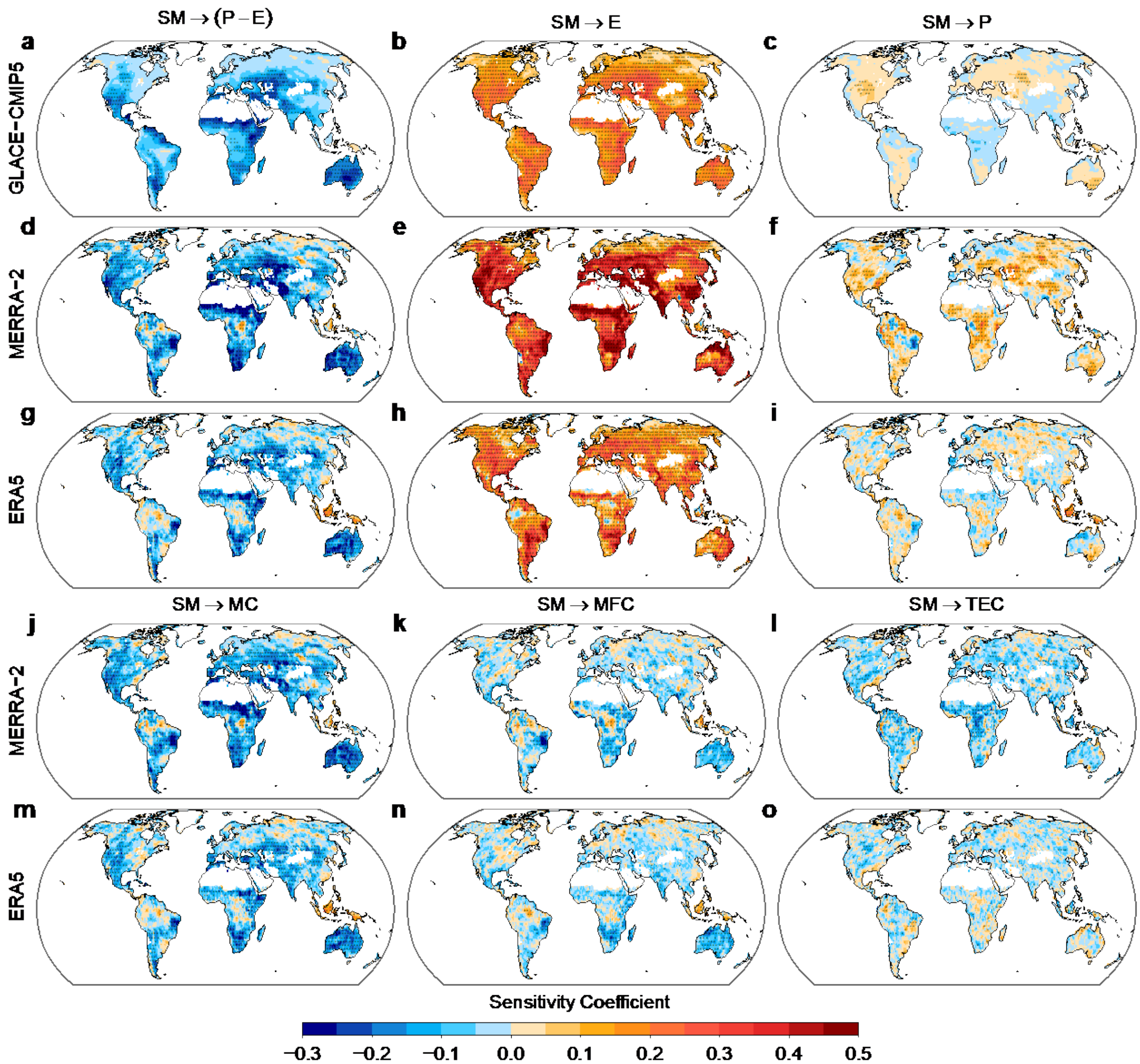

Fig. 3 | Soil moisture feedbacks on water availability in GLACE-CMIP5 models and reanalysis datasets. a-f, Sensitivity coefficients for soil moisture (SM)→precipitation minus evapotranspiration (P-E), SM→evapotranspiration (E), and SM→precipitation (P) identified based on REF of the four GLACE-CMIP5 models (1971-2100) (**a**-**c**), MERRA-2 (1980-2018) (**d**-**f**), and ERA5 (1979-2018) (**g**-**i**). Mean values of the sensitivity coefficients produced by the four models are shown in **a**-**c**. **j**-**o**, the same as **d**-**i**, but for SM→moisture convergence (MC) (**j**,**m**), SM→mean flow convergence (MFC) (**k**,**n**), and SM→transient eddy convergence (TEC) (**l**,**o**). The sensitivity coefficient for X→Y denotes the partial derivative of standardized Y to standardized X in the previous month, where the seasonal cycles and long-term trends in X and Y are removed. Stippling denotes regions where the sensitivity coefficient is significant at the 95%

level according to a bootstrap test. In **a**-**c**, stippling denotes regions where the sensitivity coefficient is significant at the 95% level and the sign of the sensitivity coefficient is consistent with the sign of multi-model means (as shown in the figure) in at least three of the four GLACE-CMIP5 models.

Although atmospheric moisture storage changes on monthly scales, the change is relatively small; thus monthly P-E approximately balances moisture convergence. The latter is calculated as the negative divergence (∇) of vertically mass-integrated moisture flux from the top of the atmosphere ($p = 0$) to the surface ($p = p_s$), i.e.,

$$P - E \approx -\frac{1}{\rho_w g} \nabla \cdot \int_0^{p_s} (\overline{\boldsymbol{u}}\overline{q} + \overline{\boldsymbol{u}' q'}) dp \qquad (1)$$

where ρ_w is the density of water, g is the acceleration due to gravity, $\boldsymbol{u}$ is the horizontal vector wind, and q is specific humidity. Moisture convergence on the right side of equation (1) is decomposed into mean flow convergence determined by monthly mean wind ($\overline{\boldsymbol{u}}$) and moisture ($\overline{q}$) fields, and transient eddy convergence associated with highly variable wind ($\boldsymbol{u}'$) and moisture (q') fields within storm systems[29,30]. We find negative SM effects on mean flow convergence and transient eddy convergence across 60-73% of the assessed land area, contributing to the negative SM→MC over more than 75% of the land area (Fig. 3j-o). As moisture flux by transient eddies is approximately diffusive[31], a negative SM influence on the transient eddy convergence may be expected based on horizontal diffusion of water vapor along specific humidity gradient into a dry air column above dry soils, but could also arise from atmospheric circulation responses.

To understand how changing SM impacts mean flow convergence, we decompose monthly variations of this quantity into a thermodynamic component induced by moisture changes ($\overline{\boldsymbol{u}}\delta\overline{q}$), a mean circulation dynamic component induced by wind changes ($\overline{q}\delta\overline{\boldsymbol{u}}$), and a covariation component by the product of monthly mean moisture and wind changes ($\delta\overline{\boldsymbol{u}}\delta\overline{q}$)[30]. The negative SM feedback on mean flow convergence arises principally from the dynamic component (Fig. 4a,f): reduced SM enhances surface heating, thereby promoting vertical ascent and associated low-level flow convergence, particularly in dry regions (see SM→negative pressure velocity in Fig. 4d,i). The dynamic component is negative across most land regions. In contrast, the SM effect on the thermodynamic component largely depends on the mean flow environment. Increasing SM increases atmospheric humidity, thus inducing greater moisture convergence (divergence) by the thermodynamic effect when the mean low-level flow is convergent (divergent) (Fig. 4b,g,e,j). This explains why the thermodynamic component of mean flow convergence acts as a positive feedback in tropical convergence zones but as a negative feedback where the mean flow is divergent. The covariation component is weaker and more spatially variable (Fig. 4c,h). Moreover, using an attribution method based on variance decomposition (Methods), we find monthly moisture convergence variations are again dominated by the dynamic component, while the contributions from other components are relatively small (Extended Data Fig. 8). These results indicate that the negative SM effect on moisture convergence and P-E are mainly determined by the SM regulation of atmospheric circulation.

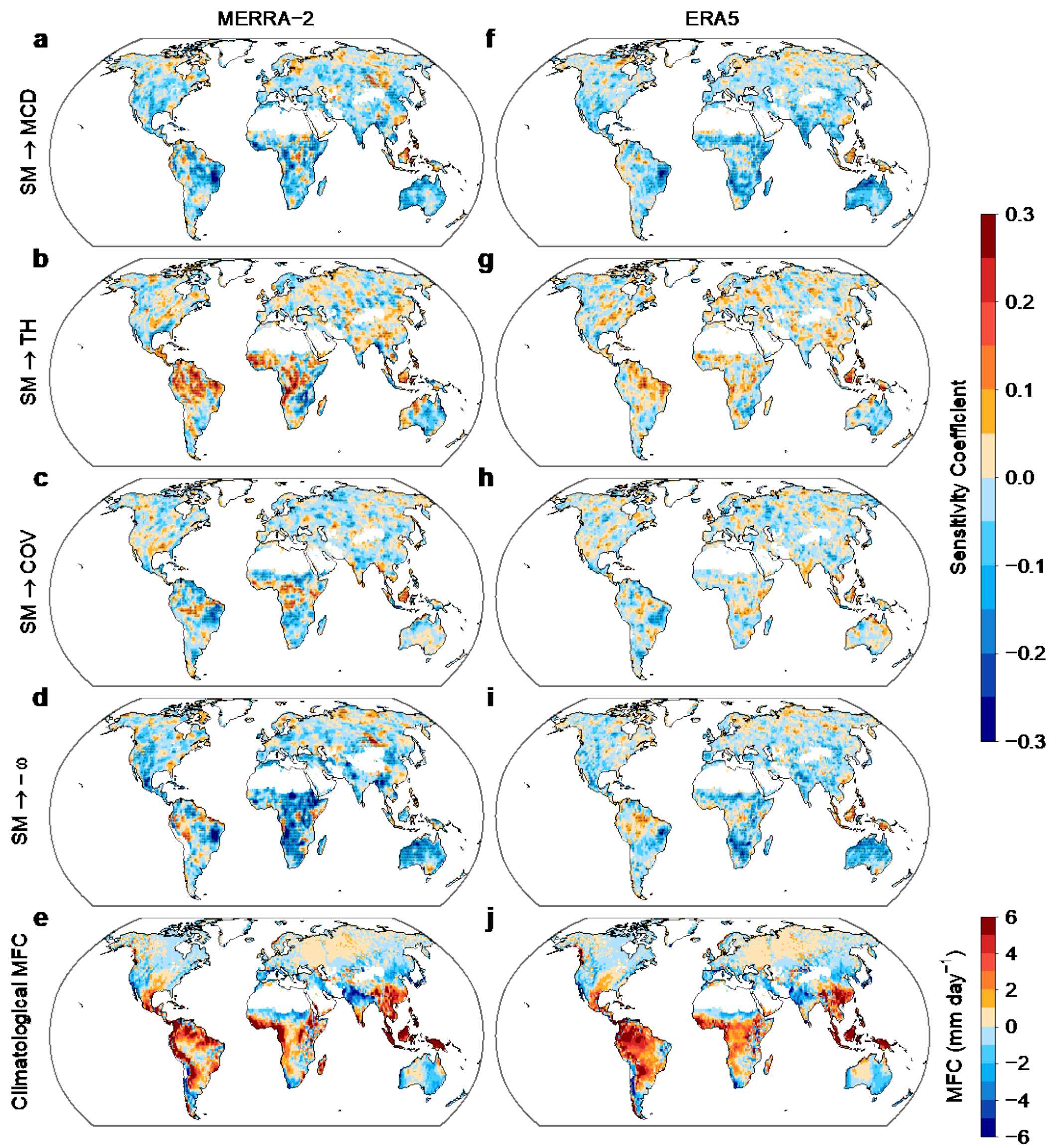

Fig. 4 | Soil moisture effects on the three components of mean flow convergence. a-e, Sensitivity coefficients for soil moisture (SM)→mean circulation dynamic component (MCD) (**a**), SM→thermodynamic component (TH) (**b**), SM→covariation component (COV) (**c**), SM→negative pressure velocity (-ω) at 700 hPa (middle troposphere) (**d**), and climatological monthly mean flow convergence (MFC) (**e**) in MERRA-2 (1980-2018). **f-j**, the same as **a-e**, but for ERA5 (1979-2018). The sensitivity coefficient for X→Y denotes the partial derivative of standardized Y to standardized X in the previous month, where the seasonal cycles and long-term trends in X and Y are removed. Stippling in **a-d** and **f-i** denotes regions where the sensitivity coefficient is significant at the 95% level according to a bootstrap test.

Discussion and implications

We demonstrate that long-term SM trends strongly influence future P-E changes, particularly over drylands. Projected reductions in dryland SM directly limit evapotranspiration and reduce moisture recycling for precipitation, but reduced SM also enhances moisture convergence, which partly counteracts precipitation declines driven by reduced evapotranspiration. These processes result in a weaker SM limitation on precipitation than on evapotranspiration, and a robust negative SM-(P-E) feedback at monthly and climatological scales. Without feedbacks from declining SM, future P-E changes would agree with the DDWW response to global warming over 31% of the land regions (Fig. 1 and Extended Data Fig. 2). However, the negative SM feedback on P-E partially offsets declines in P-E via non-SM factors over drylands, while slightly attenuating P-E increases experienced over many non-drylands, resulting in only 19% of the land regions showing the DDWW pattern.

To interpret future P-E changes over land, recent studies have emphasized the importance of land-ocean warming contrast[9,22,24], which affects the spatial pattern of atmospheric moisture content and P-E responses, in addition to local warming-driven P-E changes. The projected decline in dryland SM enhances the land-ocean warming contrast through enhanced land region warming, but thermodynamic mechanisms alone cannot well explain the negative SM feedback on P-E. Rather, we demonstrate that the negative SM-(P-E) feedback occurs mainly through SM induced changes in evapotranspiration as well as changes to the surface energy balance that modify the mean circulation, as declining SM enhances low-level vertical ascent and moisture convergence via associated low-level flow convergence. This dynamic effect may also be tied to declining SM reducing evapotranspiration and supporting a larger land-ocean warming contrast, which strengthens the landward pressure gradient and drives greater low-level moisture transport from the ocean to land[32–34].

The negative SM feedback on P-E has important implications for hydroclimatic variability[35]. From our analysis of GLACE-CMIP5 simulations, the magnitudes and frequencies of both extreme high and extreme low P-E are enhanced in the expA simulations relative to the REF (Extended Data Fig. 9). The expA simulations only include non-SM effects of oceanic and atmospheric processes, while in REF, SM variations have a positive effect on evapotranspiration but a negative feedback on moisture convergence: thus, hydroclimatic variability is muted when SM feedbacks operate. Of course, while the negative SM feedback on P-E reduces the magnitudes and frequencies of extreme P-E events in drylands, extreme hydroclimatic events, such as droughts and floods, are still projected to increase in some regions due to warming-driven ocean-atmosphere processes[36,37].

Our study highlights the importance of soil moisture changes and the associated soil moisture-atmosphere feedbacks in future projections of surface water availability. Although fully coupled general circulation models do include the negative soil moisture feedback on surface water availability over drylands, the feedback strength, as well as the soil moisture projections themselves, are highly variable and model dependent (Extended Data Fig. 3), leading to large uncertainty in how changes in soil moisture will affect future surface water availability (Fig. 1). In particular, we find that soil moisture variations contribute a larger proportion than other oceanic and atmospheric drivers (0.060 versus 0.046 mm/day, s.d. in Fig. 1h) to cross-model variations in the projected changes in dryland water availability. This points to the need for improved modelling of soil moisture trends and variability, which may be achieved through refined representation of land-atmosphere processes in general circulation models, especially the coupling between soil moisture, evapotranspiration, atmospheric circulation, and the hydrological cycle. Accurate model representation of soil moisture and the associated soil moisture-atmosphere feedbacks is crucial for providing reliable projections of surface water availability for better water resources management, and for mitigating future challenges of increasing water scarcity over drylands.

References:

1. Oki, T. & Kanae, S. Global Hydrological Cycles and World Water Resources. *Science* **313**, 1068–1072 (2006).
2. Rockström, J. *et al.* Future water availability for global food production: The potential of green water for increasing resilience to global change. *Water Resources Research* (2018) doi:10.1029/2007WR006767@10.1002/(ISSN)1944-7973.LANDUSE1.
3. Anderegg, W. R. L. *et al.* Tree mortality predicted from drought-induced vascular damage. *Nature Geosci* **8**, 367–371 (2015).
4. Ruppert, J. C. *et al.* Quantifying drylands' drought resistance and recovery: the importance of drought intensity, dominant life history and grazing regime. *Glob Change Biol* **21**, 1258–1270 (2015).
5. Huntington, T. G. Evidence for intensification of the global water cycle: Review and synthesis. *Journal of Hydrology* **319**, 83–95 (2006).
6. Held, I. M. & Soden, B. J. Robust Responses of the Hydrological Cycle to Global Warming. *J. Climate* **19**, 5686–5699 (2006).
7. Lorenz, D. J. & DeWeaver, E. T. The Response of the Extratropical Hydrological Cycle to Global Warming. *J. Climate* **20**, 3470–3484 (2007).
8. Greve, P. & Seneviratne, S. I. Assessment of future changes in water availability and aridity. *Geophysical Research Letters* **42**, 5493–5499 (2015).
9. Byrne, M. P. & O'Gorman, P. A. The Response of Precipitation Minus Evapotranspiration to Climate Warming: Why the "Wet-Get-Wetter, Dry-Get-Drier" Scaling Does Not Hold over Land. *J. Climate* **28**, 8078–8092 (2015).
10. Chou, C., Neelin, J. D., Chen, C.-A. & Tu, J.-Y. Evaluating the "Rich-Get-Richer" Mechanism in Tropical Precipitation Change under Global Warming. *J. Climate* **22**, 1982–2005 (2009).
11. Vecchi, G. A. *et al.* Weakening of tropical Pacific atmospheric circulation due to anthropogenic forcing. *Nature* **441**, 73–76 (2006).
12. Chadwick, R., Boutle, I. & Martin, G. Spatial Patterns of Precipitation Change in CMIP5: Why the Rich Do Not Get Richer in the Tropics. *J. Climate* **26**, 3803–3822 (2012).

13. Guillod, B. P., Orlowsky, B., Miralles, D. G., Teuling, A. J. & Seneviratne, S. I. Reconciling spatial and temporal soil moisture effects on afternoon rainfall. *Nature Communications* **6**, 6443 (2015).

14. Seneviratne, S. I. *et al.* Investigating soil moisture–climate interactions in a changing climate: A review. *Earth-Science Reviews* **99**, 125–161 (2010).

15. Taylor, C. M., Parker, D. J. & Harris, P. P. An observational case study of mesoscale atmospheric circulations induced by soil moisture. *Geophysical Research Letters* **34**, (2007).

16. Ookouchi, Y., Segal, M., Kessler, R. C. & Pielke, R. A. Evaluation of Soil Moisture Effects on the Generation and Modification of Mesoscale Circulations. *Mon. Wea. Rev.* **112**, 2281–2292 (1984).

17. Segal, M. & Arritt, R. w. Nonclassical Mesoscale Circulations Caused by Surface Sensible Heat-Flux Gradients. *Bull. Amer. Meteor. Soc.* **73**, 1593–1604 (1992).

18. Taylor, C. M., de Jeu, R. A. M., Guichard, F., Harris, P. P. & Dorigo, W. A. Afternoon rain more likely over drier soils. *Nature* **489**, 423–426 (2012).

19. Hsu, H., Lo, M.-H., Guillod, B. P., Miralles, D. G. & Kumar, S. Relation between precipitation location and antecedent/subsequent soil moisture spatial patterns: Precipitation-Soil Moisture Coupling. *J. Geophys. Res. Atmos.* **122**, 6319–6328 (2017).

20. Froidevaux, P., Schlemmer, L., Schmidli, J., Langhans, W. & Schär, C. Influence of the Background Wind on the Local Soil Moisture–Precipitation Feedback. *J. Atmos. Sci.* **71**, 782–799 (2013).

21. Seneviratne, S. I. *et al.* Impact of soil moisture-climate feedbacks on CMIP5 projections: First results from the GLACE-CMIP5 experiment. *Geophysical Research Letters* **40**, 5212–5217 (2013).

22. Byrne, M. P. & O'Gorman, P. A. Land–Ocean Warming Contrast over a Wide Range of Climates: Convective Quasi-Equilibrium Theory and Idealized Simulations. *J. Climate* **26**, 4000–4016 (2012).

23. Joshi, M. M., Gregory, J. M., Webb, M. J., Sexton, D. M. H. & Johns, T. C. Mechanisms for the land/sea warming contrast exhibited by simulations of climate change. *Clim Dyn* **30**, 455–465 (2008).

24. Fasullo, J. T. Robust Land–Ocean Contrasts in Energy and Water Cycle Feedbacks. *J. Climate* **23**, 4677–4693 (2010).

25. Tokinaga, H., Xie, S.-P., Deser, C., Kosaka, Y. & Okumura, Y. M. Slowdown of the Walker circulation driven by tropical Indo-Pacific warming. *Nature* **491**, 439–443 (2012).
26. Lu, J., Vecchi, G. A. & Reichler, T. Expansion of the Hadley cell under global warming. *Geophysical Research Letters* **34**, (2007).
27. Karnauskas, K. B. & Ummenhofer, C. C. On the dynamics of the Hadley circulation and subtropical drying. *Clim Dyn* **42**, 2259–2269 (2014).
28. Lau, W. K. M. & Kim, K.-M. Robust Hadley Circulation changes and increasing global dryness due to CO_2 warming from CMIP5 model projections. *Proc Natl Acad Sci USA* **112**, 3630–3635 (2015).
29. Seager, R. *et al.* Model Projections of an Imminent Transition to a More Arid Climate in Southwestern North America. *Science* **316**, 1181–1184 (2007).
30. Seager, R., Naik, N. & Vecchi, G. A. Thermodynamic and Dynamic Mechanisms for Large-Scale Changes in the Hydrological Cycle in Response to Global Warming. *J. Climate* **23**, 4651–4668 (2010).
31. O'Gorman, P. A. & Schneider, T. Stochastic Models for the Kinematics of Moisture Transport and Condensation in Homogeneous Turbulent Flows. *J. Atmos. Sci.* **63**, 2992–3005 (2006).
32. He, J. & Soden, B. J. A re-examination of the projected subtropical precipitation decline. *Nature Climate Change* **7**, 53–57 (2017).
33. Chadwick, R., Ackerley, D., Ogura, T. & Dommenget, D. Separating the Influences of Land Warming, the Direct CO2 Effect, the Plant Physiological Effect, and SST Warming on Regional Precipitation Changes. *Journal of Geophysical Research: Atmospheres* **124**, 624–640 (2019).
34. Findell, K. L. *et al.* Rising Temperatures Increase Importance of Oceanic Evaporation as a Source for Continental Precipitation. *Journal of Climate* **32**, 7713–7726 (2019).
35. Krakauer, N. Y., Cook, B. I. & Puma, M. J. Contribution of soil moisture feedback to hydroclimatic variability. *Hydrol. Earth Syst. Sci.* 16 (2010).
36. Roudier, P. *et al.* Projections of future floods and hydrological droughts in Europe under a +2°C global warming. *Climatic Change* **135**, 341–355 (2016).

37. Zhou, S., Zhang, Y., Williams, A. P. & Gentine, P. Projected increases in intensity, frequency, and terrestrial carbon costs of compound drought and aridity events. *Science Advances* **5**, eaau5740 (2019).

Materials and Methods

CMIP5 model simulations. We used 35 CMIP5 models (listed in Table S1) covering the historical (1971-2000) and future (2071-2100, RCP8.5 high emissions scenario) periods. The ensemble member "r1i1pi" was used for each model. These models were selected because they provide the monthly total soil moisture content, precipitation, and latent heat flux required for our analyses. Evapotranspiration was calculated from latent heat flux in each model. We calculated multi-model mean annual changes in these variables between the historical and future periods.

GLACE-CMIP5 experiments. We used simulations from four models (i.e., EC-EARTH, ECHAM6, GFDL and IPSL) that participate in the GLACE-CMIP5 experiment, which was performed to assess the impact of SM-climate feedbacks in CMIP5 projections[21] and has been widely used to isolate the SM effect on the atmosphere[38–40]. We did not use the other two models (ACCESS and CCSM4) in the GLACE-CMIP5 experiment because of problems with the prescribed SM. In each model, we used three simulations, i.e., a reference simulation (REF) and two perturbation simulations (expB and expA), covering the period from 1950 to 2100. All three simulations were driven by prescribed sea surface temperature, sea ice, land use, and CO_2 concentrations from the respective CMIP5 simulations (the historical simulations over 1950-2005 and the RCP8.5 scenario over 2006-2100). The difference between the three simulations is that SM was fully coupled with the atmosphere in REF, while SM climatology was prescribed as the 1971-2000 climatology (expA) and a centered, 30-year running mean climatology from REF (expB) in the two perturbation simulations (Extended Data Fig. 1). Comparing simulated atmospheric variables between the three simulations, we could isolate the effects of SM trends (expB-expA) and variability (REF-expB) and total SM effect (REF-expA) due to SM-atmosphere feedbacks.

For our analyses, we used monthly total soil moisture content, precipitation, and latent heat flux from the three simulations in each model. Evapotranspiration was calculated from latent heat flux in each simulation. Multi-model mean annual changes in SM between the historical and future periods in REF were compared with those from CMIP5. In each model, we calculated mean annual changes in precipitation, evapotranspiration, and P-E between the historical and future periods in the three simulations. We isolated the contributions of total SM changes (REF-expA), SM trends (expB-expA), and SM variability (REF-expB) to future changes in these variables. To investigate the mechanisms behind the SM effect on P-E changes, we used near-surface (2m) temperature, specific humidity, and the vertical profile of pressure velocity from expA and expB. Temperature is available in all four models, but specific humidity is not archived in EC-EARTH, and pressure velocity is only available in IPSL.

Reanalysis datasets. To identify the SM feedback on P-E, we used monthly root-zone SM, precipitation, evapotranspiration from the Modern-Era Retrospective analysis for Research and Applications, version 2 (MERRA-2)[41] dataset (1980-2018), and the European Centre for Medium-Range Weather Forecasts (ERA5, 1979-2018). In ERA5, we used 0-100cm SM to approximate root-zone SM. As the two reanalysis datasets are constrained by *in situ* and satellite remote sensing observations, they largely reflect the relationship between SM and P-E. However, these reanalysis datasets prescribe monthly climatology of leaf area index based on satellite products. Because vegetation dynamics generally amplify SM-driven evapotranspiration and precipitation anomalies in dry regions[42], lack of such effects may thus dampen simulated SM-atmosphere feedbacks in reanalysis products.

To further understand how SM impacts P-E, we used vertically integrated moisture convergence (MC) and decomposed MC into mean flow convergence and transient eddy convergence, using monthly specific humidity and eastward and northward wind at all pressure levels (0-1000 hPa), and surface pressure from ERA5 and MERRA2 (see "Moisture Convergence Decomposition" below). We also used monthly pressure velocity at 700 hPa, which provides a good representation of the middle tropospheric circulation, from ERA5 and MERRA2 to assess the SM effect on atmospheric vertical motion.

Definition of drylands. Drylands are generally defined as regions with an aridity index (the ratio of precipitation to potential evapotranspiration, P/E_0) less than 0.65[43]. There are numerous ways to estimate E_0 under certain climatic conditions[44], which may result in varying definitions of drylands. A good E_0 estimation can well predict mean annual evapotranspiration (E) through the Budyko functions[45]. A widely used analytical Budyko function[46] is

$$\frac{E}{P} = \frac{1}{\left[\left(\frac{E_0}{P}\right)^{-n} + 1\right]^{\frac{1}{n}}} \tag{2}$$

The parameter n represents the influence of land characteristics on E. Comparing existing Budyko functions, the Pike's equation (n=2.0) is closest to the original Budyko curve[45]. Using the Pike's equation to describe the relationship between E/P and E_0/P, we obtained a E/P ratio of 0.84 when P/E_0 is set as the threshold of 0.65. In other words, drylands are identified as regions where E/P is greater than 0.84. Noting that climate models do not produce E_0, but do simulate E and P, we therefore defined drylands as regions where multi-model mean E/P is larger than 0.84 in the historical period (1971-2000) for CMIP5 and GLACE-CMIP5 (REF) models (Extended Data Fig. 2a,c).

The SM-(P-E) feedback. Because SM and P-E are strongly coupled, it is difficult to isolate the SM feedback on P-E from the direct P-E impact on SM. A feedback has been quantified based on the temporally lagged correlation in many previous studies[47,48]. The difficulty in determining the SM-(P-E) feedback is mainly because of the persistent impact of P-E (especially P) on SM, as the slow processes of soil water percolation, evaporation, and transpiration lead to relatively long SM memory (weeks to months) of precipitation events[49]. The lagged correlation between SM and subsequent P-E therefore may reflect precipitation autocorrelation rather than the SM-(P-E) feedback[47]. Additionally, the seasonal cycles and long-term trends of P-E and SM also contribute to the lagged correlation[47], although they are largely driven by external factors such as regional climatology and global warming.

To address these issues, we established a multiple linear regression model between P-E and one-month lagged SM to assess the SM-(P-E) feedback.

$$(P-E)_d(t+1) = n_0 + n_1 \cdot SM_d(t) + n_2 \cdot (P-E)_d(t) \tag{3}$$

The subscript d indicates that the multi-year mean seasonal cycle and the linear trend of the variable have been removed, and the indicator t represents monthly steps. The lagged term

$(P-E)_d(t)$ on the right side of equation (3) aims to remove the effect of P-E autocorrelation. Therefore, the regression coefficient n_1 ($\frac{\partial (P-E)_d(t+1)}{\partial SM_d(t)}$) represents the SM feedback on P-E. Although the SM-(P-E) feedback may be non-linear and time-dependent, the regression coefficient obtained from the linear model reflects the long-term mean effect of SM on P-E.

We used partial least square regression (PLSR)[50] to obtain the regression coefficient n_1 in equation (3). PLSR combines features of principal component analysis and multiple linear regression (MLR). It projects the predictor variables onto orthogonal principal components to overcome the issue of multicollinearity among predictor variables (i.e., the predictor variables are highly linearly related). PLSR then regresses the dependent variable against principal components to obtain regression slopes. We find that $(P-E)_d(t)$ and $SM_d(t)$ are weakly correlated in most grid cells. In these cases, PLSR obtains the same regression results as MLR. In case of a strong correlation between $(P-E)_d(t)$ and $SM_d(t)$ at some grid cells, we use PLSR instead of MLR to overcome the multicollinearity problem. To facilitate comparison of the SM-(P-E) feedback across different regions and in different datasets/models, we used PLSR standardized coefficients (or dimensionless sensitivity coefficients) corresponding to standardized $(P-E)_d$ and SM_d of zero mean and unit variance (z-score) to measure the SM-(P-E) feedback.

As the SM-(P-E) feedback may be impacted by natural variability, we used a bootstrap test to determine the significance of the sensitivity coefficients. We performed bootstrap analyses with 500 realizations for the two reanalysis datasets (480 months for ERA5 and 468 months for MERRA-2) and 2000 realizations for fully coupled simulations of the four GLACE-CMIP5 models (1560 months, 1971-2100). The time series are randomly resampled to obtain the 95% confidence intervals of the sensitivity coefficients. We used the adjusted bootstrap percentile interval as different types of confidence intervals generate very similar results. According to the bootstrap confidence intervals, the sensitivity coefficients are deemed to be statistically significant if the 95% confidence intervals do not contain zero.

We also used similar multiple linear regression models and bootstrap tests to assess the SM feedbacks on evapotranspiration and precipitation. To demonstrate that the SM-atmosphere feedbacks are consistent between current and future climates, we used data from the fully coupled

GLACE-CMIP5 simulations to compare the SM-atmosphere feedbacks: (1) between recent (1979-2018) and future (2061-2100) periods, and (2) by removing and retaining the long-term trends in the variables during the 1971-2100 period. Both comparisons show consistent strong positive SM→E, weak SM→P, and negative SM→(P-E) (Fig. 3a-c and Extended Data Fig. 10). In particular, the spatial correlation coefficient for SM→(P-E) is 0.92 in comparison (1) and 0.97 in comparison (2), indicating that the negative SM-(P-E) feedback is robust to the presence of long-term climate change.

Moisture Convergence Decomposition. Atmospheric MC is calculated as the negative divergence of vertically integrated moisture flux over the pressure (p) from the top of the atmosphere ($p = 0$) to the surface ($p = p_s$).

$$MC = -\frac{1}{\rho_w g} \nabla \cdot \int_0^{p_s} (\boldsymbol{u} q) dp \quad (4)$$

ρ_w is the density of water, g is the acceleration due to gravity, ∇ is the horizontal divergence operator, $\boldsymbol{u}$ is the horizontal vector wind, and q is specific humidity.

At the monthly scale, MC can be decomposed into mean flow convergence (MFC) determined by atmospheric mean wind and moisture fields and transient eddy convergence (TEC) by highly variable (hourly to daily) wind and moisture fields within storm systems[29].

$$MC = -\frac{1}{\rho_w g} \nabla \cdot \int_0^{p_s} (\overline{\boldsymbol{u}}\overline{q} + \overline{\boldsymbol{u}'q'}) dp \quad (5)$$

$$MFC = -\frac{1}{\rho_w g} \nabla \cdot \int_0^{p_s} (\overline{\boldsymbol{u}}\overline{q}) dp \quad (6)$$

$$TEC = -\frac{1}{\rho_w g} \nabla \cdot \int_0^{p_s} (\overline{\boldsymbol{u}'q'}) dp \quad (7)$$

Overbars indicate monthly mean values, and primes represent departures from the monthly mean values.

Using climatological monthly values of $\overline{\boldsymbol{u}}$ and $\overline{q}$ as reference, monthly MFC anomalies (δMFC) can be further decomposed into three components[30]: 1) a thermodynamic component (δTH) induced by specific humidity anomalies, 2) a mean circulation dynamic component (δMCD)

induced by horizontal wind anomalies, and 3) a covariation component (δCOV) induced by the product of specific humidity anomalies and horizontal wind anomalies.

$$\delta MFC = -\frac{1}{\rho_w g}\nabla \cdot \int_0^{p_s} (\bar{\boldsymbol{u}}_0 \delta \bar{q} + \bar{q}_0 \delta \bar{\boldsymbol{u}} + \delta \bar{\boldsymbol{u}} \delta \bar{q}) dp \tag{8}$$

$$\delta TH = -\frac{1}{\rho_w g}\nabla \cdot \int_0^{p_s} (\bar{\boldsymbol{u}}_0 \delta \bar{q}) dp \tag{9}$$

$$\delta MCD = -\frac{1}{\rho_w g}\nabla \cdot \int_0^{p_s} (\bar{q}_0 \delta \bar{\boldsymbol{u}}) dp \tag{10}$$

$$\delta COV = -\frac{1}{\rho_w g}\nabla \cdot \int_0^{p_s} (\delta \bar{\boldsymbol{u}} \delta \bar{q}) dp \tag{11}$$

The subscript 0 represents climatological monthly values and δ represents departure from the monthly climatology.

Attribution analysis. We used a variance decomposition method[51,52] to assess contributions of each MC component to monthly variations in MC. We removed the long-term trends and seasonal cycles to focus on the sub-seasonal and inter-annual variations in MC.

$$MC_d = MFC_d + TEC_d \tag{12}$$

As in equation (3), the subscript d indicates the variable is linearly detrended and deseasonalized. The variance of MC_d ($var(MC_d)$) can be decomposed into its covariance with the two components on the right side of equation (12).

$$var(MC_d) = cov(MC_d, MFC_d) + cov(MC_d, TEC_d) \tag{13}$$

The contributions of MFC_d ($R(MC, MFC)$) and TEC_d ($R(MC, TEC)$) to MC_d variations in MERRA2 (1980-2018) and ERA5 (1979-2018) are therefore calculated as

$$R(MC, MFC) = \frac{cov(MC_d, MFC_d)}{var(MC_d)} \tag{14}$$

$$R(MC, TEC) = \frac{cov(MC_d, TEC_d)}{var(MC_d)} \tag{15}$$

Similarly, we assessed contributions of the three components of MFC_d to MC_d variations. The separated contributions of MFC_d, TEC_d and the three components of MFC_d to MC_d variations are shown in Extended Data Fig. 8.

Data availability. The GLACE-CMIP5 simulations are available from S.I.S. (sonia.seneviratne@ethz.ch) and the climate modelling groups upon reasonable request. All other data used in this study are available online. The CMIP5 model simulations are from https://esgf-node.llnl.gov/search/cmip5/. The ERA5 reanalysis data are from https://www.ecmwf.int/en/forecasts/datasets/archive-datasets/reanalysis-datasets/era5. The MERRA-2 reanalysis data are from https://gmao.gsfc.nasa.gov/reanalysis/MERRA-2/data_access/. The source data for the figures are publicly available (https://doi.org/10.6084/m9.figshare.12982880).

Code availability. The code used for modelling and reanalysis data analyses is publicly available (https://doi.org/10.5281/zenodo.4041736).

References

38. Lorenz, R. *et al.* Influence of land-atmosphere feedbacks on temperature and precipitation extremes in the GLACE-CMIP5 ensemble. *Journal of Geophysical Research: Atmospheres* **121**, 607–623 (2016).

39. Berg, A. *et al.* Land–atmosphere feedbacks amplify aridity increase over land under global warming. *Nature Climate Change* **6**, 869–874 (2016).

40. Zhou, S. *et al.* Land–atmosphere feedbacks exacerbate concurrent soil drought and atmospheric aridity. *PNAS* 201904955 (2019) doi:10.1073/pnas.1904955116.

41. Gelaro, R. *et al.* The Modern-Era Retrospective Analysis for Research and Applications, Version 2 (MERRA-2). *J. Climate* **30**, 5419–5454 (2017).

42. Green, J. K. *et al.* Regionally strong feedbacks between the atmosphere and terrestrial biosphere. *Nature Geoscience* **10**, 410–414 (2017).

43. Huang, J., Yu, H., Guan, X., Wang, G. & Guo, R. Accelerated dryland expansion under climate change. *Nature Climate Change* **6**, 166–171 (2016).

44. Milly, P. C. D. & Dunne, K. A. Potential evapotranspiration and continental drying. *Nature Climate Change* **6**, 946–949 (2016).

45. Zhou, S., Yu, B., Huang, Y. & Wang, G. The complementary relationship and generation of the Budyko functions. *Geophysical Research Letters* **42**, 1781–1790 (2015).

46. Choudhury, BhaskarJ. Evaluation of an empirical equation for annual evaporation using field observations and results from a biophysical model. *Journal of Hydrology* **216**, 99–110 (1999).

47. Wei, J., Dickinson, R. E. & Chen, H. A Negative Soil Moisture–Precipitation Relationship and Its Causes. *J. Hydrometeor.* **9**, 1364–1376 (2008).

48. Zhang, J., Wang, W.-C. & Wei, J. Assessing land-atmosphere coupling using soil moisture from the Global Land Data Assimilation System and observational precipitation. *J. Geophys. Res.* **113**, D17119 (2008).

49. Seneviratne, S. I. *et al.* Soil Moisture Memory in AGCM Simulations: Analysis of Global Land–Atmosphere Coupling Experiment (GLACE) Data. *J. Hydrometeor.* **7**, 1090–1112 (2006).

50. Geladi, P. & Kowalski, B. R. Partial least-squares regression: a tutorial. *Analytica Chimica Acta* **185**, 1–17 (1986).

51. Zhou, S. *et al.* Sources of Uncertainty in Modeled Land Carbon Storage within and across Three MIPs: Diagnosis with Three New Techniques. *J. Climate* **31**, 2833–2851 (2018).

52. Zhou, S. *et al.* Response of Water Use Efficiency to Global Environmental Change Based on Output From Terrestrial Biosphere Models: Drivers of WUE Variability. *Global Biogeochemical Cycles* **31**, 1639–1655 (2017).

Correspondence Statement

Correspondence and requests for materials should be addressed to S.Z..

Acknowledgements

We acknowledge the World Climate Research Programme's Working Group on Coupled Modelling, which is responsible for CMIP, and we thank the climate modeling groups (listed in Table S1 of this paper) for producing and making available their model output. For CMIP the U.S. Department of Energy's Program for Climate Model Diagnosis and Intercomparison provides coordinating support and led development of software infrastructure in partnership with the Global Organization for Earth System Science Portals. S.Z. acknowledges support from the Lamont-

Doherty Postdoctoral Fellowship and the Earth Institute Postdoctoral Fellowship. P.G. acknowledges support from NASA ROSES Terrestrial hydrology (NNH17ZDA00IN-THP) and NOAA MAPP NA17OAR4310127. A.P.W. and B.I.C. acknowledge support from the NASA Modeling, Analysis, and Prediction (MAP) program (NASA 80NSSC17K0265). T.F.K. acknowledges support from the RUBISCO SFA, which is sponsored by the Regional and Global Model Analysis (RGMA) Program in the Climate and Environmental Sciences Division (CESD) of the Office of Biological and Environmental Research (BER) in the U.S. Department of Energy Office of Science, and additional support from a DOE Early Career Research Program award #DE-SC0021023. We also acknowledge Richard Seager and Jason Smerdon from Lamont-Doherty Earth Observatory of Columbia University for insightful discussion and techincal assistance with and interpretation of the moisture convergence decomposition (R.S.). LDEO contribution number is 8453.

Author contributions

S.Z. conceived and designed the study. S.Z. processed model simulations and reanalysis data. S.Z., A.P.W., B.R.L., A.M.B., Y.Z., T.F.K., B.I.C., S.H., S.I.S. and P.G. contributed to data analysis and interpretation. S.Z. drafted the manuscript. All authors edited the manuscript.

Competing interests

The authors declare no competing interests.

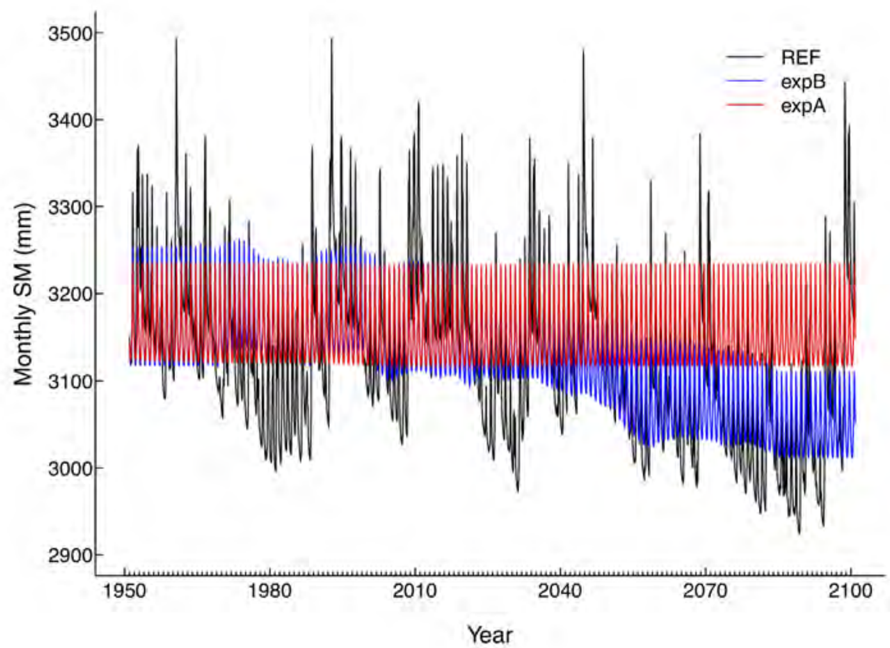

Extended Data Fig. 1 | Illustration of total column monthly soil moisture (SM) in the three simulations in GLACE-CMIP5. SM data shown in the figure are obtained from a grid cell in the GFDL model.

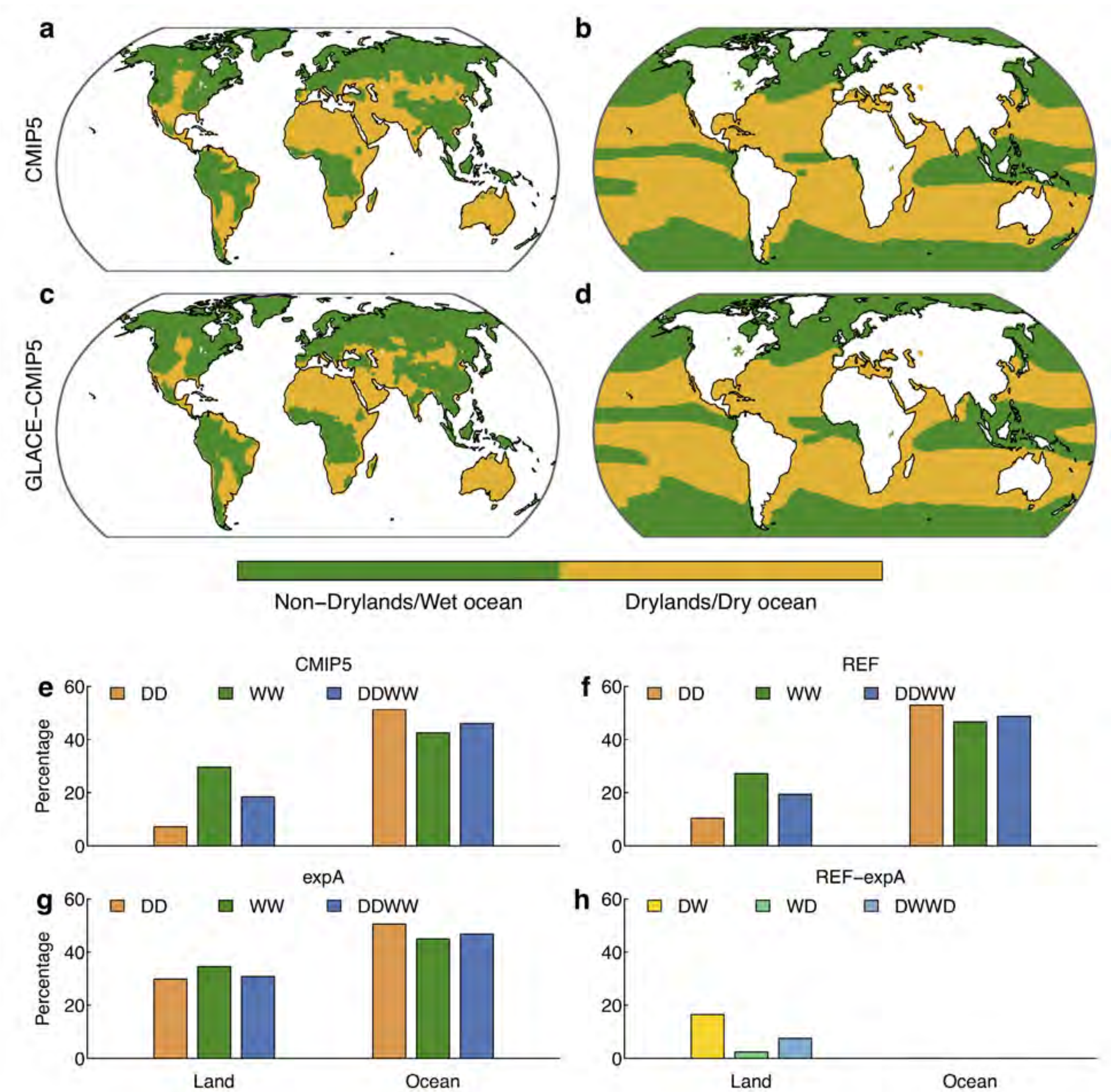

Extended Data Fig. 2 | Global distribution of dry and wet regions and assessment of the "dry-get-drier, and wet-get-wetter" paradigm. a-d, Global distribution of dry and wet regions in CMIP5 models (**a-b**), and GLACE-CMIP5 models (**c-d**). **e-h**, Percentages of the dry and wet regions that show significant P-E changes in CMIP5 and GLACE-CMIP5 in Fig. 1. DD (WW) represents the percentage of dry (wet) regions that show significant P-E declines (increases). DW (WD) represents the percentage of dry (wet) regions that show significant P-E increases (decreases). DDWW (DWWD) represents the percentage of land or ocean regions with DD and WW (DW and WD). Antarctica is excluded from the land regions.

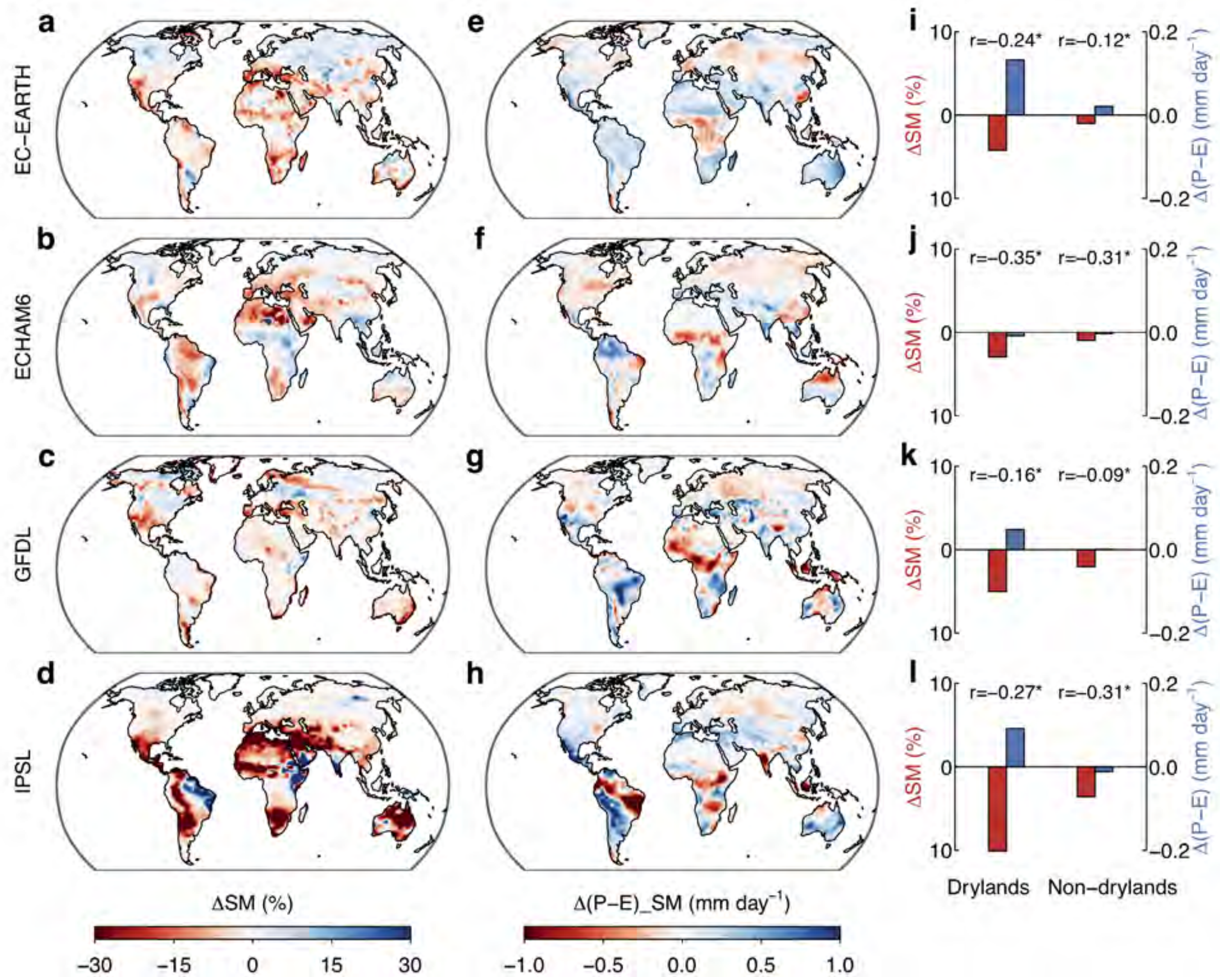

Extended Data Fig. 3 | Future SM changes and associated P-E changes in the four GLACE-CMIP5 models. a-d, Percent changes in SM between historical (1971-2000) and future (2071-2100) periods. **e-h**, Future changes in P-E induced by SM changes. **i-l**, Mean changes in SM and P-E for the drylands and non-drylands. The spatial correlation coefficient (r) between changes in SM and P-E over the drylands (left) and non-drylands (right) are also shown. All the correlation coefficients are statistically significant at the 0.001(*) level following the Student's t-test.

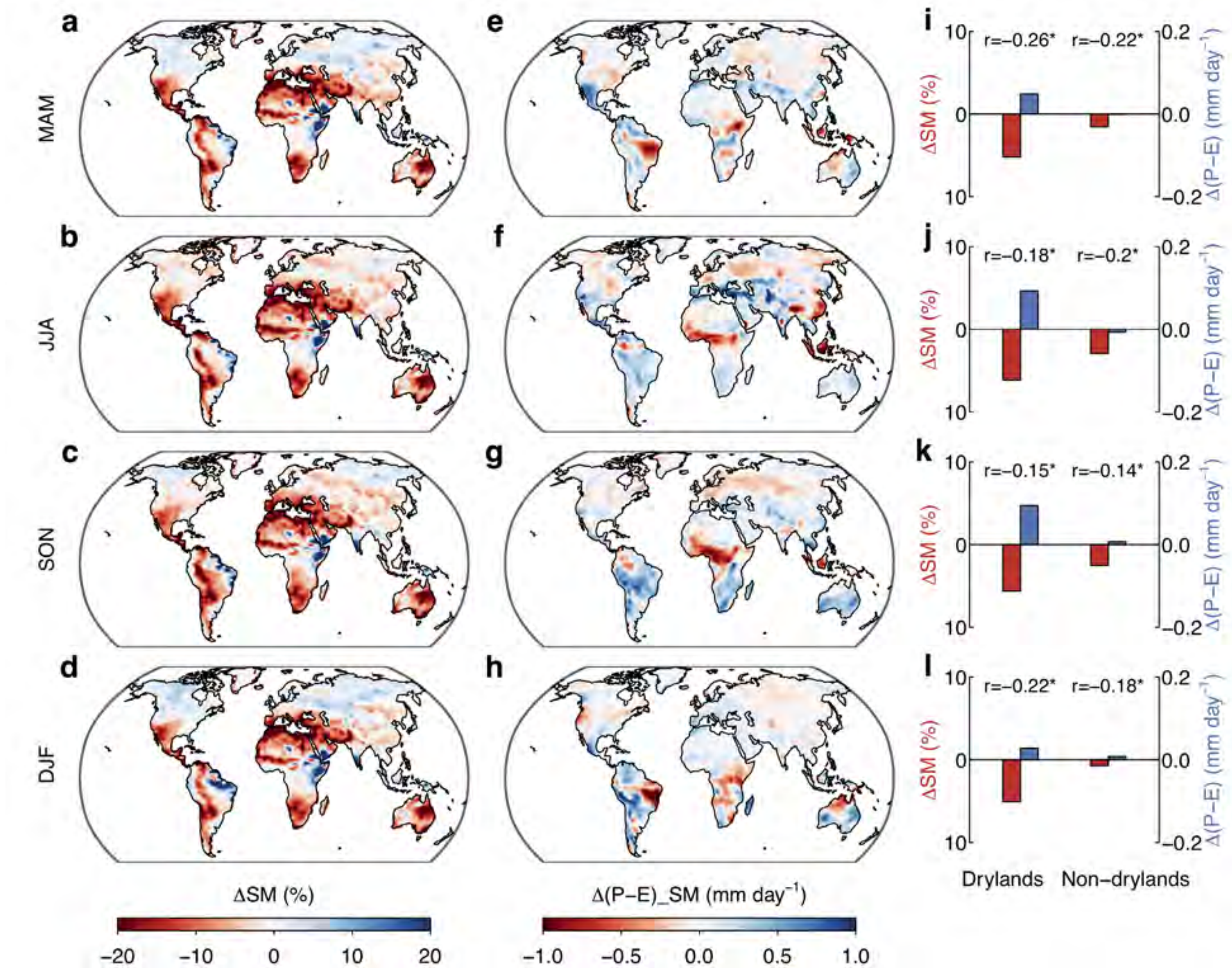

Extended Data Fig. 4 | Future SM changes and associated P-E changes for each season in GLACE-CMIP5. a-d, Multi-model mean percent changes in SM between historical (1971-2000) and future (2071-2100) periods in the four seasons. **e-h**, Mean changes in P-E induced by SM changes. **i-l**, Mean changes in SM and P-E for the drylands and non-drylands. The spatial correlation coefficient (r) between changes in SM and P-E over the drylands (left) and non-drylands (right) are also shown. All the correlation coefficients are statistically significant at the 0.001(*) level following the Student's t-test.

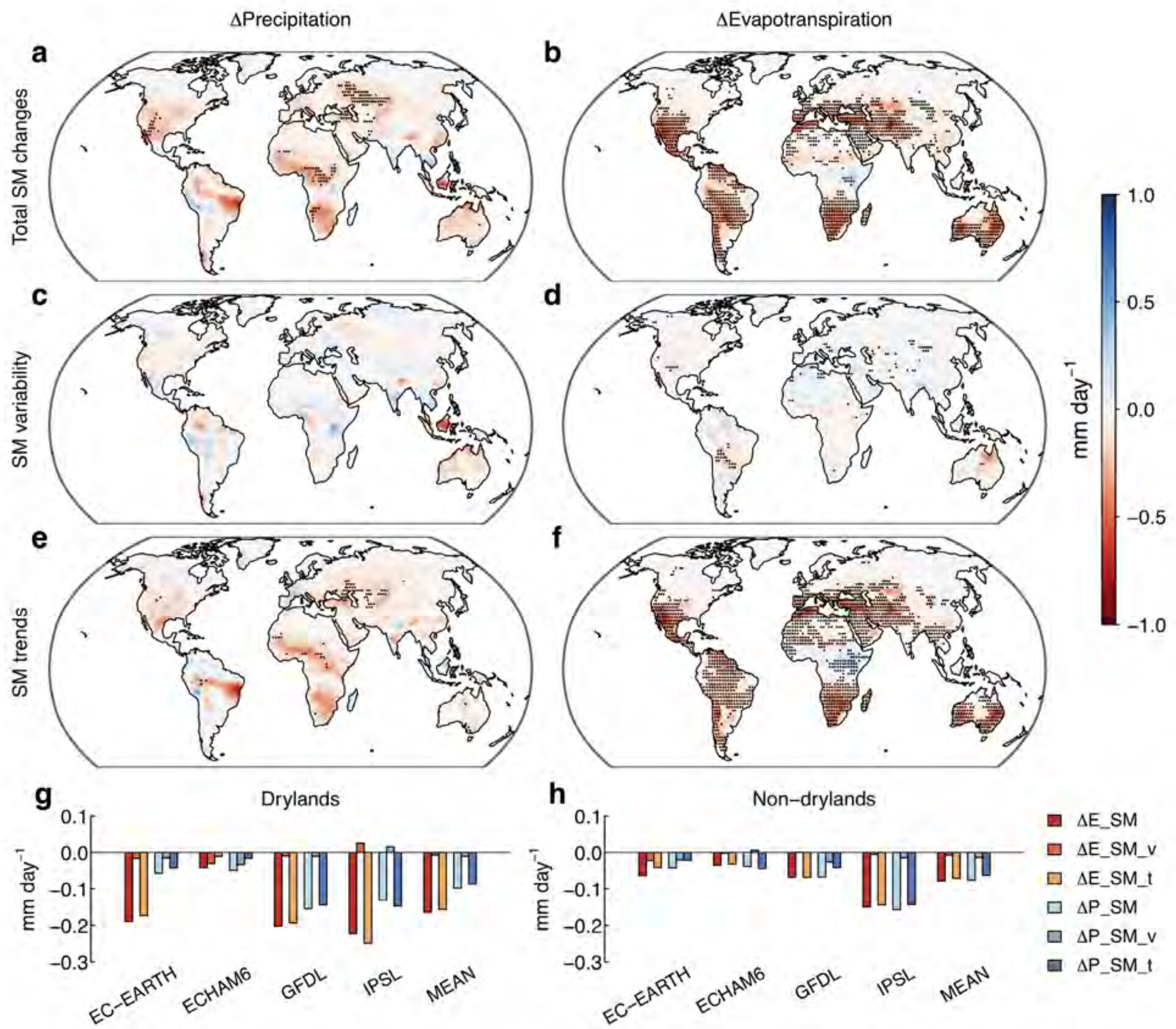

Extended Data Fig. 5 | SM impacts on precipitation and evapotranspiration changes in the four GLACE-CMIP5 models. a-b, SM induced changes (Δ) in precipitation (**a**) and evapotranspiration (**b**) between historical (1971-2000) and future (2071-2100) periods (future minus historical values). **c-f**, The same as **a-b**, but for the effects of SM variability (**c-d**) and SM trends (**e-f**). **g-h**, Contributions of total SM changes, SM variability (SM_v), and SM trends (SM_t) to precipitation and evapotranspiration changes across drylands (**g**) and non-drylands (**h**) in the four models. Stippling denotes regions where the changes in precipitation and evapotranspiration are significant at the 95% level (Student's t-test) and the sign of the change is consistent with the sign of multi-model means (as shown in the figures) in at least three of the four models.

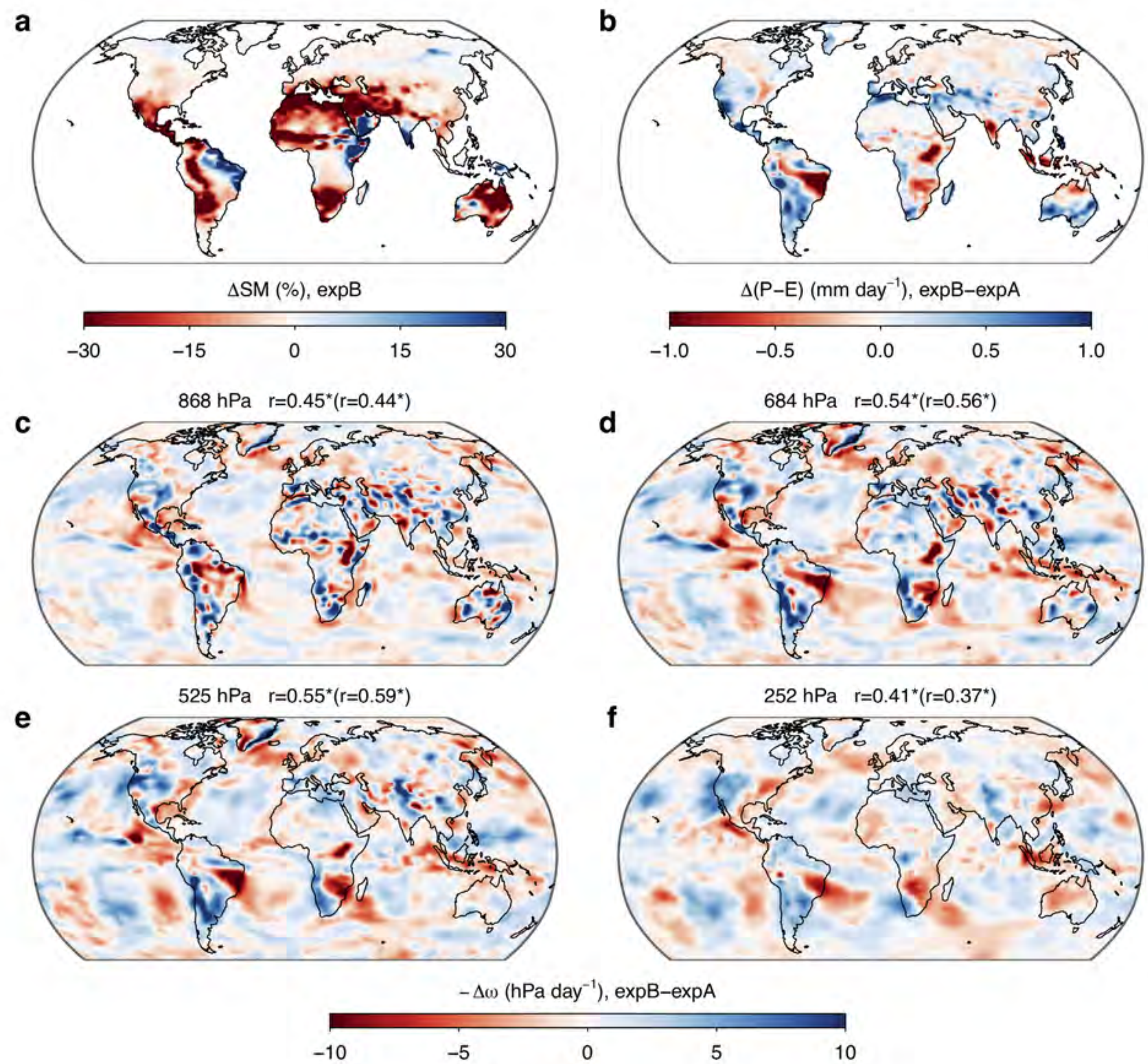

Extended Data Fig. 6 | Soil moisture effects on vertical ascent in the IPSL model. a, Percent changes of SM in expB (SM trends) between historical (1971-2000) and future (2071-2100) periods. **b**, Future changes in P-E induced by SM trends (expB-expA). **c**-**f**, Changes in the spatial pattern of negative pressure velocity (-Δω, expB-expA) at different pressure levels of the troposphere. The spatial correlation coefficient between changes in P-E and negative pressure velocity over land (drylands in parentheses) are also shown in **c**-**f**. All the correlation coefficients are statistically significant at the 0.001(*) level following the Student's t-test.

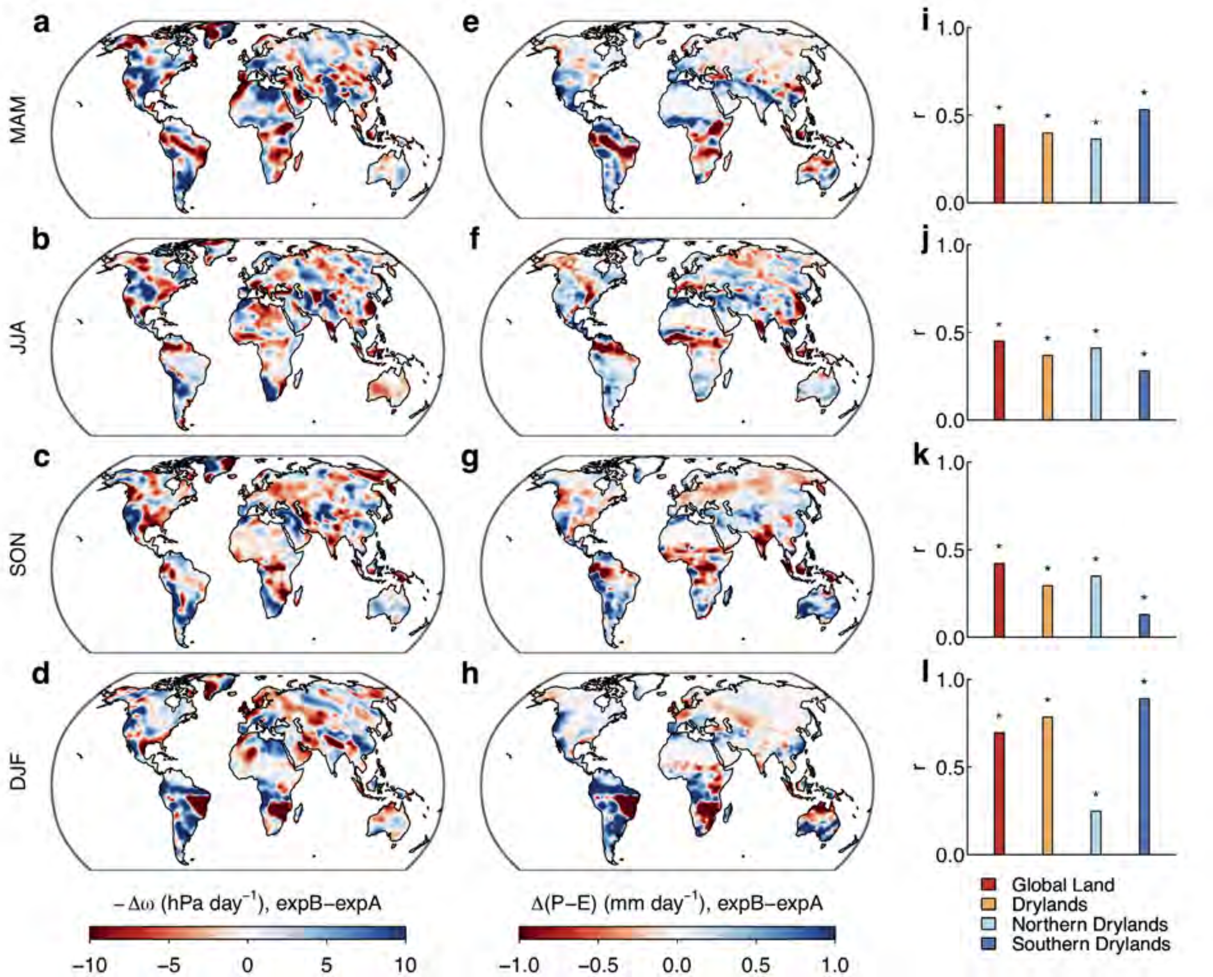

Extended Data Fig. 7 | Soil moisture effects on vertical ascent for each season in the IPSL model. a-h, Spatial patterns of future changes in negative pressure velocity (-Δω, 525 hPa, **a-d**) and P-E (**e-h**) between historical (1971-2000) and future (2071-2100) periods due to SM trends (expB-expA) in the four seasons. **i-l**, Spatial correlation coefficients between future changes in P-E and negative pressure velocity over land and drylands. All the correlation coefficients are statistically significant at the 0.001(*) level following the Student's t-test.

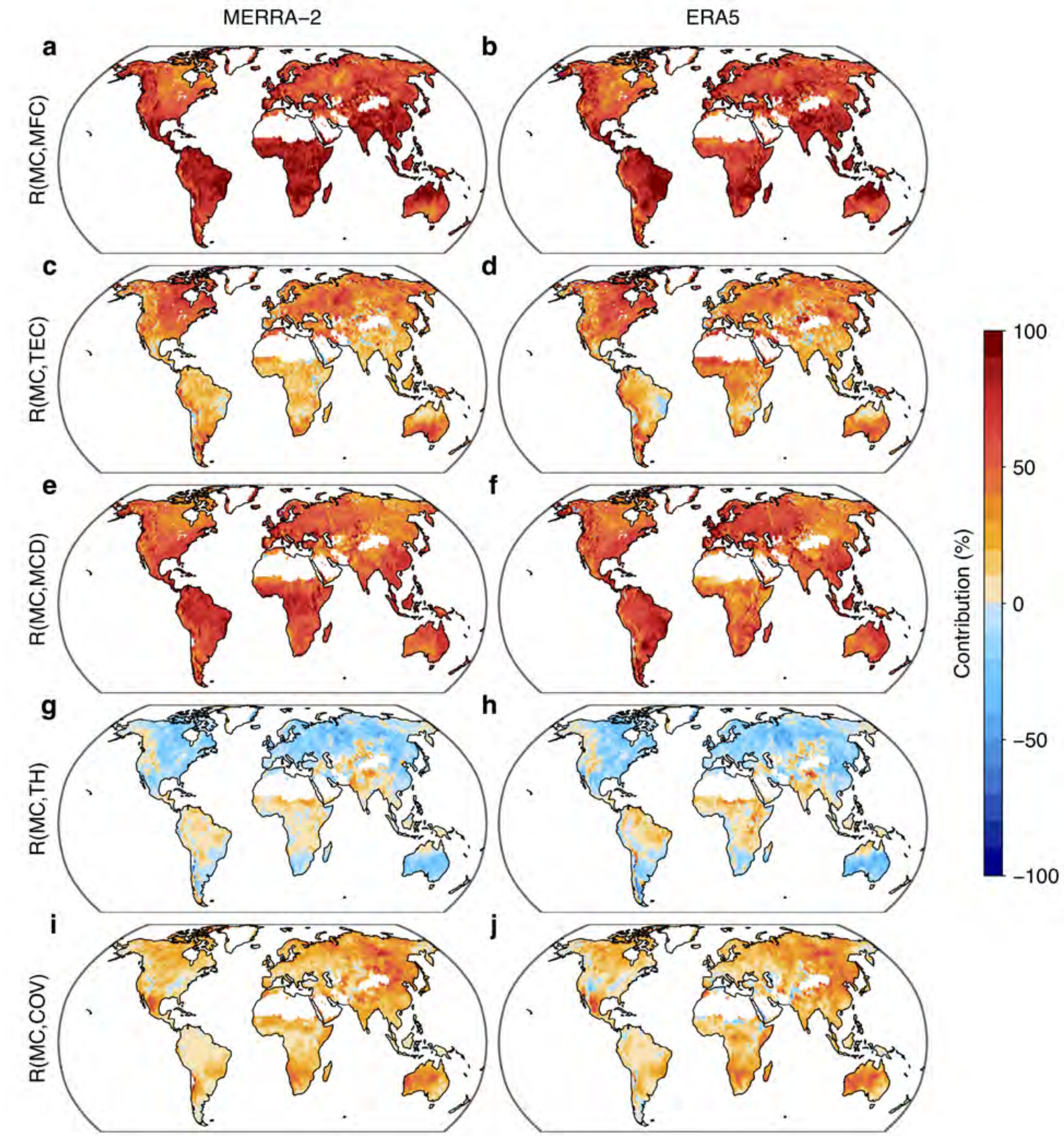

Extended Data Fig. 8 | Contributions of each component to moisture convergence variations. **a**,**b**, Contribution of the mean flow convergence to moisture convergence variations (R(MC,MFC)) in MERRA-2 (1980-2018) and ERA5 (1979-2018). **c**-**j**, The same as **a**,**b**, but for contributions of the transient eddy convergence (R(MC,TEC)) (**c**,**d**), the mean circulation dynamic component (R(MC,MCD)) (**e**,**f**), the thermodynamic component (R(MC,TH)) (**g**,**h**), and the covariation component (R(MC,COV)) (**i**,**j**).

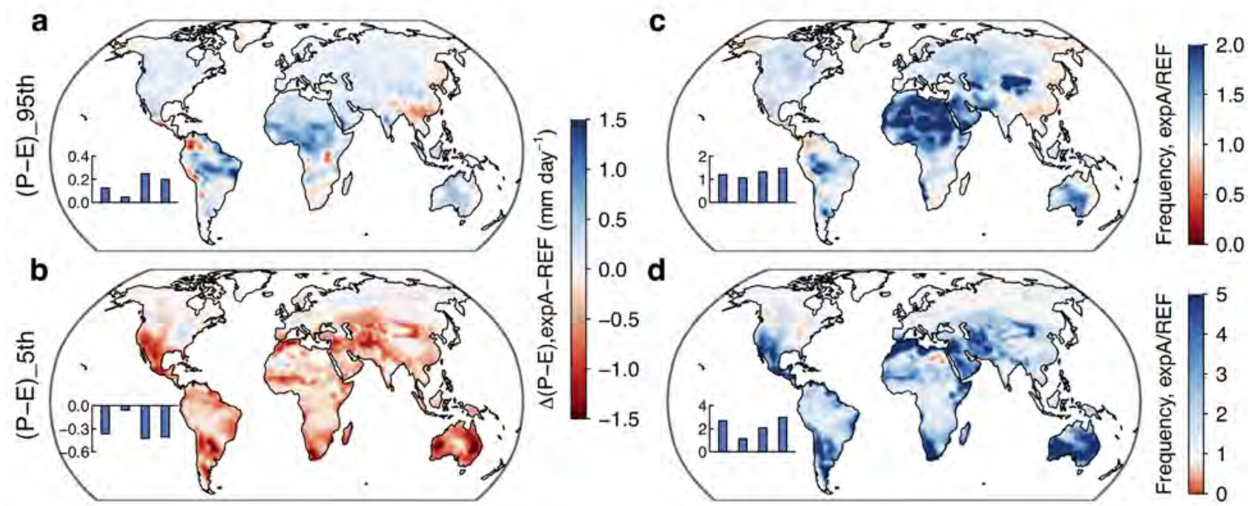

Extended Data Fig. 9 | Multi-model mean differences in monthly P-E extremes between expA and REF in GLACE-CMIP5. a-b, Differences in 95th percentile P-E (**a**), and 5th percentile P-E (**b**) between expA and REF over the period of 1950-2100. **c-d**, Ratio of the frequency of extreme high P-E (above 95th percentile P-E in REF) (**c**) and extreme low P-E (below 5th percentile P-E in REF) (**d**) between expA and REF. The inset barplots show area-weighted means for the four models (EC-EARTH, ECHAM6, GFDL, IPSL) in GLACE-CMIP5.

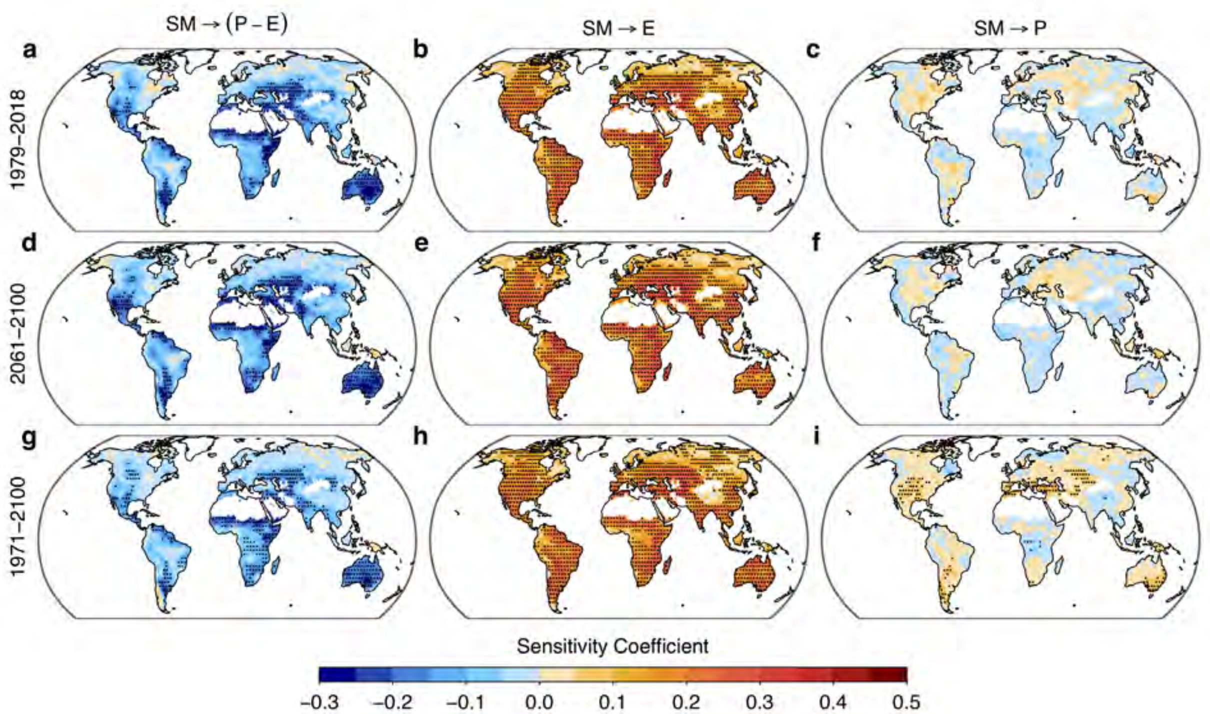

Extended Data Fig. 10 | Soil moisture feedbacks on water availability in GLACE-CMIP5 models. Mean sensitivity coefficients for soil moisture (SM)→precipitation minus evapotranspiration (P-E), SM→evapotranspiration (E) and SM→precipitation (P) identified based on REF of the four GLACE-CMIP5 models during 1979-2018 (**a**-**c**), 2061-2100 (**d**-**f**) and 1971-2100 (**g**-**i**). The sensitivity coefficient for X→Y denotes the partial derivative of standardized Y to standardized X in the previous month, where the seasonal cycles and long-term trends in X and Y are removed (**a**-**f**). In **g**-**i**, the seasonal cycles of X and Y are removed but the trends in X and Y are retained. Stippling denotes regions where the sensitivity coefficient is significant at the 95% level according to a bootstrap test and the sign of the sensitivity coefficient is consistent with the sign of multi-model means (as shown in the figure) in at least three of the four GLACE-CMIP5 models.

Table S1. List of the 35 CMIP5 models (historical and RCP8.5 simulations) used in this study.

Model Name	Institute ID	Modeling Center
ACCESS1-0	CSIRO-BOM	Commonwealth Scientific and Industrial Research Organization (CSIRO) and Bureau of Meteorology CSIRO-BOM (BOM), Australia
ACCESS1-3		
bcc-csm1-1	BCC	Beijing Climate Center, China Meteorological Administration
bcc-csm1-1-m		
BNU-ESM	GCESS	College of Global Change and Earth System Science, Beijing Normal University
CanESM2	CCCMA	Canadian Center for Climate Modeling and Analysis
CCSM4	NCAR	National Center for Atmospheric Research
CESM1-BGC	NSF-DOE-NCAR	Community Earth System Model Contributors
CMCC-CM	CMCC	Centro Euro-Mediterraneo per I Cambiamenti Climatici
CMCC-CMS		
CNRM-CM5	CNRM-CERFACS	Centre National de Recherches Météorologiques / Centre Européen de Recherche et Formation Avancée en Calcul Scientifique
CSIRO-Mk3-6-0	CSIRO-QCCCE	Commonwealth Scientific and Industrial Research Organization in collaboration with Queensland Climate Change Centre of Excellence
GFDL-CM3	NOAA GFDL	NOAA Geophysical Fluid Dynamics Laboratory
GFDL-ESM2G		
GFDL-ESM2M		
GISS-E2-H	NASA GISS	NASA Goddard Institute for Space Studies
GISS-E2-H-CC		
GISS-E2-R		
GISS-E2-R-CC		
HadGEM2-AO	NIMR/KMA	National Institute of Meteorological Research/Korea Meteorological Administration
HadGEM2-CC	MOHC (additional realizations by INPE)	Met Office Hadley Centre (additional HadGEM2-ES realizations contributed by Instituto Nacional de Pesquisas Espaciais)
HadGEM2-ES		
inmcm4	INM	Institute for Numerical Mathematics
IPSL-CM5A-LR	IPSL	Institut Pierre Simon Laplace
IPSL-CM5A-MR		

IPSL-CM5B-LR		
MIROC5	MIROC	Atmosphere and Ocean Research Institute (The University of Tokyo), National Institute for Environmental Studies, and Japan Agency for Marine-Earth Science and Technology
MIROC-ESM	MIROC	Japan Agency for Marine-Earth Science and Technology, Atmosphere and Ocean Research Institute (The University of Tokyo), and National Institute for Environmental Studies
MIROC-ESM-CHEM		
MPI-ESM-LR	MPI-M	Max Planck Institute for Meteorology
MPI-ESM-MR		
MRI-CGCM3	MRI	Meteorological Research Institute
MRI-ESM1		
NorESM1-M	NCC	Norwegian Climate Centre
NorESM1-ME		